

Characterization of a Nitric Oxide Synthase from the Plant Kingdom: NO Generation from the Green Alga *Ostreococcus tauri* Is Light Irradiance and Growth Phase Dependent

Noelia Foresi,^{a,1} Natalia Correa-Aragunde,^{a,1} Gustavo Parisi,^b Gonzalo Caló,^c Graciela Salerno,^c and Lorenzo Lamattina^{a,2}

^a Instituto de Investigaciones Biológicas, Facultad de Ciencias Exactas y Naturales, Universidad Nacional de Mar del Plata, 7600 Mar del Plata, Argentina

^b Centro de Estudios e Investigaciones, Universidad Nacional de Quilmes, Sáenz Peña 180, B1876BXD Bernal, Argentina

^c Centro de Investigaciones Biológicas and Centro de Estudios de Biodiversidad y Biotecnología de Mar del Plata, Fundación para Investigaciones Biológicas Aplicadas, 7600 Mar del Plata, Argentina

The search for a nitric oxide synthase (NOS) sequence in the plant kingdom yielded two sequences from the recently published genomes of two green algae species of the *Ostreococcus* genus, *O. tauri* and *O. lucimarinus*. In this study, we characterized the sequence, protein structure, phylogeny, biochemistry, and expression of NOS from *O. tauri*. The amino acid sequence of *O. tauri* NOS was found to be 45% similar to that of human NOS. Folding assignment methods showed that *O. tauri* NOS can fold as the human endothelial NOS isoform. Phylogenetic analysis revealed that *O. tauri* NOS clusters together with putative NOS sequences of a *Synechococcus* sp strain and *Physarum polycephalum*. This cluster appears as an outgroup of NOS representatives from metazoa. Purified recombinant *O. tauri* NOS has a K_m for the substrate L-Arg of $12 \pm 5 \mu\text{M}$. *Escherichia coli* cells expressing recombinant *O. tauri* NOS have increased levels of NO and cell viability. *O. tauri* cultures in the exponential growth phase produce 3-fold more NOS-dependent NO than do those in the stationary phase. In *O. tauri*, NO production increases in high intensity light irradiation and upon addition of L-Arg, suggesting a link between NOS activity and microalgal physiology.

INTRODUCTION

Nitric oxide (NO) is a ubiquitous intra- and intercellular messenger that functions in many physiological processes in all kingdoms of life. In animals, NO is produced by the enzyme nitric oxide synthase (NOS; EC 1.14.13.39). NOS catalyzes the formation of NO and citrulline from L-Arg in a reaction that requires NADPH as an electron donor and O_2 as a cosubstrate. Three NOS isoforms have been described in animals: the constitutive neuronal NOS (nNOS), endothelial NOS (eNOS), and the inducible NOS (iNOS) (Alderton et al., 2001). NOS is a bimodal enzyme, comprising an N-terminal oxygenase domain (NOSoxy) that binds protoporphyrin IX (heme), 6R-tetra-hydrobiopterin (H_4B), L-Arg, and a C-terminal reductase domain (NOSred) that binds the cofactors flavin mononucleotide (FMN), flavin adenine dinucleotide (FAD), and NADPH. The two domains are connected by a calmodulin (CaM) binding sequence. The activity of the two

constitutive NOS isoforms is dependent on changes in the concentration of intracellular Ca^{2+} , whereas iNOS is Ca^{2+} -CaM independent (Griffith and Stuehr, 1995).

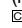
Genomic and functional analyses indicate that NOS enzymes are present in organisms ranging from bacteria to humans (Gorren and Mayer, 2007). Gram-positive bacteria encode smaller NOS proteins, containing only the oxygenase domain. Bacterial NOS uses nonspecific cellular reductases to produce NO (Wang et al., 2007; Gusarov et al., 2008). In higher plants, there are at least two enzymatic sources of NO production: (1) nitrate reductase, which reduces nitrate to nitrite, and then nitrite to NO (Yamasaki et al., 1999); and (2) a NOS-like enzymatic activity (Corpas et al., 2009). Even though the existence of a plant NOS remains a matter of debate, it has been inferred from measurements of NOS activity in several plant extracts (Cueto et al., 1996; Barroso et al., 1999; Caro and Puntarulo, 1999; Ribeiro et al., 1999; Corpas et al., 2009) and inhibition of NO production using mammalian NOS inhibitors (Cueto et al., 1996; Bright et al., 2006; Valderrama et al., 2007). A recent article focused on the relevance of NOS-derived NO metabolism in plant plastids (Gas et al., 2009). However, no gene or protein with sequence similarity to animal or bacterial NOSs has been reported for plants.

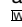
The green alga *Ostreococcus tauri* is the smallest-known free-living eukaryote and is an abundant picoeukaryotic group throughout the oceanic zone. This organism belongs to the Prasinophyceae (Chlorophyta), a primitive class within the green

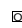
¹ These authors contributed equally to this work.

² Address correspondence to lolama@mdp.edu.ar.

The author responsible for distribution of materials integral to the findings presented in this article in accordance with the policy described in the Instructions for Authors (www.plantcell.org) is: Lorenzo Lamattina (lolama@mdp.edu.ar).

 Some figures in this article are displayed in color online but in black and white in the print edition.

 Online version contains Web-only data.

 Open Access articles can be viewed online without a subscription. www.plantcell.org/cgi/doi/10.1105/tpc.109.073510

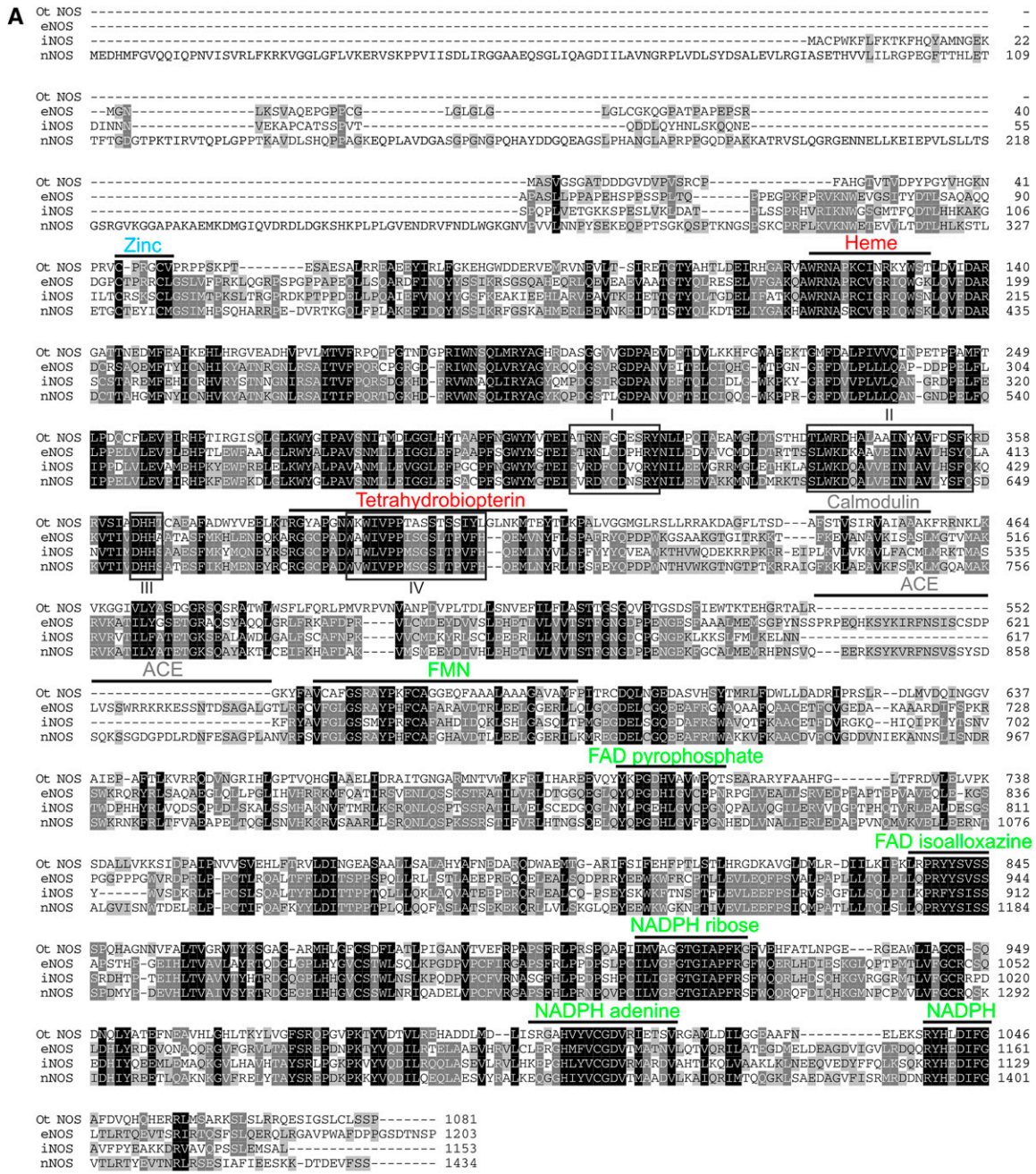


Figure 1. Alignment of *O. tauri* NOS (Ot NOS) and Human NOS Sequences.

plant lineage that evolved after the endosymbiosis event that gave rise to photosynthetic eukaryotes (Díez et al., 2001). The recent sequencing of the *O. tauri* genome revealed that it has one of the smallest (12.56 Mb) and most compact nuclear genomes known to date (Derelle et al., 2006). This single-celled alga is of particular interest because it shares a common ancestor with higher plants and is considered to be an early-diverging class within the green plant lineage. Studying the genes that algae and higher plants have in common and analyzing how they have evolved and are regulated could provide insight into their functions. These features make *O. tauri* a potentially powerful biological model to study fundamental cellular processes and gene evolution in photosynthetic eukaryotes.

In this work, we report the functional characterization of the NOS enzyme from *O. tauri* by heterologous expression in *Escherichia coli*, prediction of its structural arrangement, and determination of its kinetic parameters and spectroscopic properties. Bacteria carrying the NOS gene display enhanced NO production and cell viability. *O. tauri* expresses NOS throughout its life cycle, but NO production is highest at the exponential growth phase and increases during high intensity light irradiance. Thus, this report describes a NOS enzyme from the plant kingdom that has most of the characteristics ascribed to animal NOS.

RESULTS

Sequence and Structural Analysis of *O. tauri* NOS

The NOS sequence was obtained from the published genome sequence of *O. tauri*. The amino acid sequence was predicted and annotated as a NOS enzyme (Derelle et al., 2006). Interpro and PFAM searches were used to identify conserved domains in the primary sequence, and the NOS was found to contain the characteristic NOSoxy and NOSred domains (Sheta et al., 1994; Lowe et al., 1996). These findings were also supported by the fold assignment results using HHPred and FFAS03, where a NOSoxy (PDB code 1d0c with a score of -89.00 ; a score of less than -9.5 is significant) and a NOSred domain (PDB code 1tll with a score of -132.00) were found. Figure 1A shows the *O. tauri* NOS (Ot NOS) sequence alignment with human eNOS, iNOS, and nNOS. The similarity between segments of aligned Ot NOS and human eNOS that overlap is 44%, whereas that between Ot NOS and both iNOS and nNOS is 45%. Full-length sequence similarity is 41.6, 42.7, and 34.3% for eNOS, iNOS, and nNOS, respectively. Furthermore, binding regions of the heme group and cofactors

H₄B, FMN, FAD, and NADPH are largely conserved among all sequences (Figures 1A and 1B). The first 90 residues are divergent with respect to other NOS enzymes, except for a putative zinc binding motif. *O. tauri* NOS contains a C-(x)₃-C motif (where C is Cys and x any residue) instead of the C-(x)₄-C zinc binding motif commonly found in animal NOS enzymes (Figure 1A; Alderton et al., 2001). Although the putative CaM binding site is not well conserved in *O. tauri* NOS, the CaM binding region seems to correspond to the classical Ca²⁺-dependent 1-5-8-14 motif, based on the positions of conserved hydrophobic residues (Rhoads and Friedberg, 1997). Furthermore, an analysis using HHPred (Söding et al., 2005) established that this region is similar to the CaM binding region of nNOS from *Gallus gallus* (PDB code 2o60, E-value 0.0036). The regions involved in the dimerization interface of NOS proteins (i.e., regions I, II, III, and IV) (Bird et al., 2002) are also conserved (Figure 1A).

Structural models based on best templates from FFAS03 and HHPred results were built using MODELLER. Figures 2A and 2B show the estimated three-dimensional structure of the *O. tauri* NOSoxy domain based on the coordinates of *Bos taurus* eNOSoxy. The model was assessed for quality with PROSA II (Wiederstein and Sippl, 2007) and resulted in a z-score of -9.06 , which is similar to that of *B. taurus* eNOS (z-score -9.36). The cofactor and substrate binding sites in the *O. tauri* NOSoxy and *B. taurus* eNOSoxy structures are almost identical (Figures 2A and 2B, insets). Furthermore, the residues that interact with the substrate L-Arg, the cofactor H₄B, and heme are fully conserved in the *O. tauri* NOS sequence (Figure 2C). NOS belongs to the family of Cys-coordinated heme proteins in which the proximal ligand to the heme-Fe is the sulfur atom of an intrinsic Cys residue (Rousseau et al., 2005). In *O. tauri* NOS, heme is stabilized by bonding to the sulfur atom of Cys-125 (Figure 2C). The substrate L-Arg above the heme iron atom is stabilized by a H-bonding network involving Trp-301, Tyr-302, and Glu-306 that interact with the terminal nitrogen atom, terminal oxygen atom, and guanidium nitrogen, respectively (Figure 2C). L-Arg and H₄B are linked together by a H-bond that is mediated by one of the two propionate groups of the heme. H₄B is further stabilized by an interaction with the oxygen of the Trp-392 residue (Figure 2C).

The predicted structure of *O. tauri* NOSred is also conserved among NOSred domains from animals. Figure 2D shows the superposition of *O. tauri* NOSred and *Rattus norvegicus* nNOSred and reveals two main differences between the domains. Ot NOS does not contain the autoinhibitory control element (ACE) that blocks the electron flow in the absence of CaM (Figure 1A; Salerno et al., 1997). The C2DA loop contributes

Figure 1. (continued).

(A) The sequences of Ot NOS and human eNOS, nNOS, and iNOS were aligned using ClustalX and Genedoc software. Black boxes indicate conserved residues in all four sequences, dark-gray boxes represent conserved residues in three sequences, and light-gray boxes represent conserved residues in two sequences. Amino acids that share no similarity are unshaded. Putative cofactor binding sites for zinc, Heme, H₄B, CaM, FMN, FAD pyrophosphate, FAD isoalloxazine, NADPH ribose, NADPH adenine, and the C-terminal domain of NADPH are shown. Regions involved in the dimerization interface (i.e., regions I, II, III, and IV) are boxed.

(B) Comparison of the domain architecture of NOS from different sources. Eukaryotic NOS enzymes have a Zn binding region, a NOSoxy domain that binds heme, L-Arg, and H₄B, a CaM binding region, and a NOSred domain with subdomains that bind FMN, FAD, and NAD. Bacterial NOS enzymes contain only a NOSoxy domain. The question mark indicates that the Zn binding motif is not completely conserved. H₄B/THF means that it is not clear whether NOS-containing bacteria synthesize H₄B, although they can use tetrahydrofolate (THF) as a pterin cofactor (Crane et al., 2010).

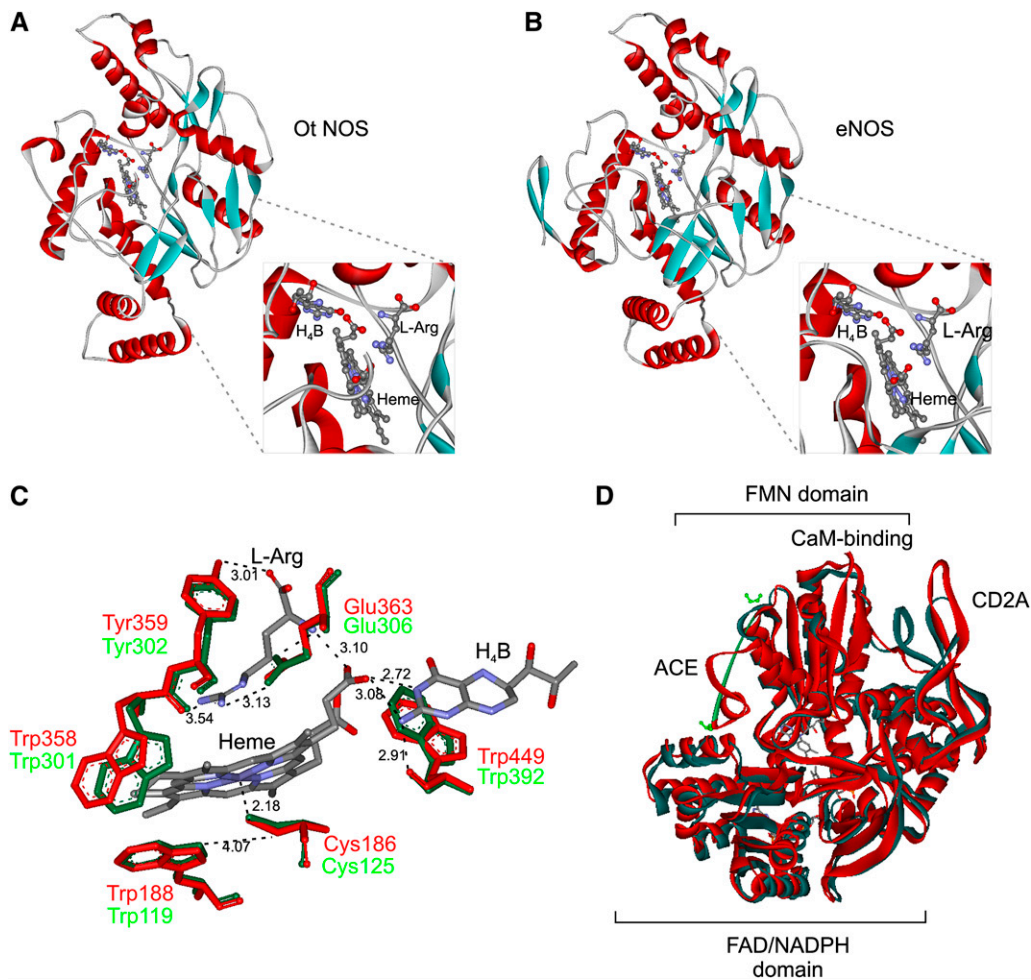


Figure 2. Predicted Structure of Oxygenase (NOSoxy) and Reductase (NOSred) Domains from *O. tauri* NOS.

(A) and (B) Ribbon diagram of Ot NOSoxy (A) generated according to the coordinates of the crystallized eNOSoxy of *B. taurus* (B). Inset: Magnified region showing the catalytic site of NOS, which contains heme, H₄B, and L-Arg.

(C) Superposition of residues in the active site of Ot NOS (green) and eNOS (red). Hydrogen bonds are indicated as dotted lines.

(D) Structural alignment between model of Ot NOSred (green) and nNOSred from *R. norvegicus* (red). Ot NOS contains a shorter CD2A loop and lacks the ACE segment. Note that the nNOS structure represented lacks part of the ACE segment. Due to the high motility of the ACE segment, it was not modeled; therefore, residues Ser-849 to Gly-872 are not depicted. The first and last residues Ser-849 and Gly-872 of the crystal structure of nNOS are shown in ball and stick in light green.

to the Ca²⁺ dependence of CaM-bound activity (Knudsen et al., 2003) and is shorter in *O. tauri* NOSred than in nNOSred (Figure 2D).

Phylogenetic Analysis of *O. tauri* NOS

BLAST searches against the protein nonredundant database from GenBank were used to collect close putative homologs of *O. tauri* NOS. The sequences retrieved mainly belonged to the superkingdom Eukaryota and to the Metazoa kingdom. Few exceptions were found, such as a NOS from Amoebozoa (*Physarum polycephalum*), from bacteria (*Synechococcus* sp), and from the close homolog *Ostreococcus lucimarinus*. Figure 3 (see Supplemental Data Set 1 online) shows the majority-rule

consensus tree obtained from 1000 replicates of maximum likelihood trees. The numbers near the internal nodes in the figure indicate the relative support resulting from nonparametric bootstrapping. Nodes with bootstrap values of below 40% were collapsed. The tree can be divided into two main divisions. A major cluster contains the three NOS isoforms from vertebrate organisms (in red in Figure 3). The clustering pattern within this group represents functional diversification of NOS types (eNOS, nNOS, and iNOS) (Figure 3). The second populated cluster contains NOS from invertebrates (phyla Placozoa, Cnidaria, Arthropoda, and Mollusca). In this cluster, we also found representatives from green algae (*O. tauri* and *O. lucimarinus*), bacteria (*Synechococcus* sp), and Amoebozoa (*P. polycephalum*), which are well established outgroups of the Metazoa kingdom

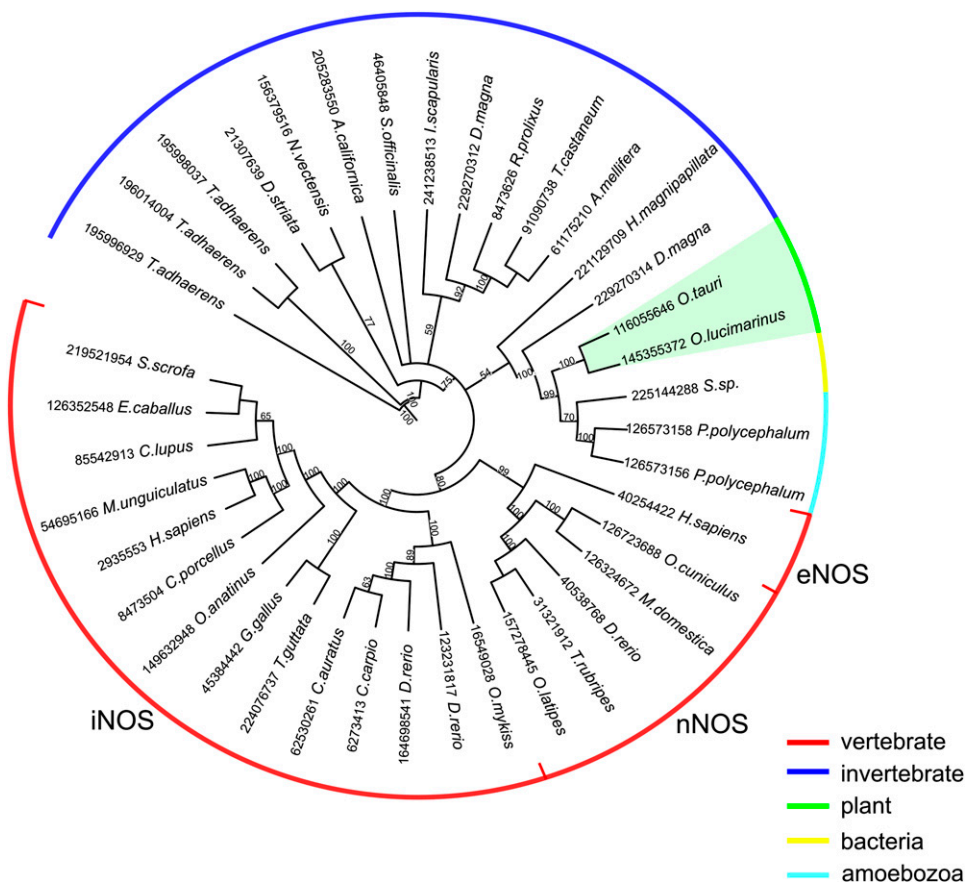


Figure 3. Phylogenetic Tree of NOS Sequences.

Radial representation of consensus maximum likelihood tree obtained from 1000 replicates using the JTT+F+Gamma model. Colors indicate main taxonomic divisions: vertebrates (red), invertebrates (blue), plants (green), bacteria (yellow), and amoebzoa (light blue). The accession number of each sequence is given next to the species name. Values in the branches indicate bootstrap percentage. Bootstrap values below 40% are not shown.

(Adoutte et al., 2000). While the clustering pattern among these organisms is well supported, their insertion in the cluster containing other metazoan representatives (in blue in Figure 3) is not adequately supported, making it difficult to establish deep evolutionary relationships among the NOS enzymes within the cluster.

Expression and Purification of Recombinant *O. tauri* NOS

Recombinant *O. tauri* NOS expressed in *E. coli* appeared as a 119-kD band on an SDS-PAGE gel (Figure 4A, lane 2), in agreement with the molecular mass expected from the amino acid sequence. *E. coli* cells transformed with the empty vector did not contain proteins in this mass region (Figure 4A, lane 1). NOS was purified using 2'-5'-ADP agarose column chromatography. The purified protein migrated as a single band on an SDS-PAGE gel (Figure 4A, lane 3) and exhibited immunoreactivity with anti-OtNOS antibody (Figure 4B). Under the conditions described in Methods, 1 to 2 mg of recombinant NOS protein was purified from 1 liter of transgenic *E. coli* BI21 cell culture expressing pET24b-OtNOS.

Changes in the heme pocket architecture of purified recombinant protein after the addition of different ligands were monitored by the spectral perturbation effect. Spectra exhibit a broad peak at λ 396 nm (Figure 4C), which is typical of the presence of a high-spin heme prosthetic group. The addition of 1 mM imidazole resulted in the complete conversion of the heme group to a low-spin state, characterized by a peak at λ 487 nm. After the formation of the imidazole-NOS complex, the addition of L-Arg resulted in a shift of absorbance maximum at λ 410 nm, supporting the reconversion of the heme iron to the high-spin state (Figure 4C).

Catalytic Activity of Recombinant *O. tauri* NOS

The activity of purified recombinant NOS was assessed by two methods: (1) NO production by the oxyhemoglobin capture assay and (2) [3 H]L-citrulline formation (Table 1). Using the oxyhemoglobin assay, we observed a prolonged burst phase of NO release (\sim 150 s at $0.49 \pm 0.03 \mu\text{M NO min}^{-1}$) in reactions containing L-Arg, the cofactor H₄B, and CaM, followed by an extended period of slower NO release (33% of the initial phase).

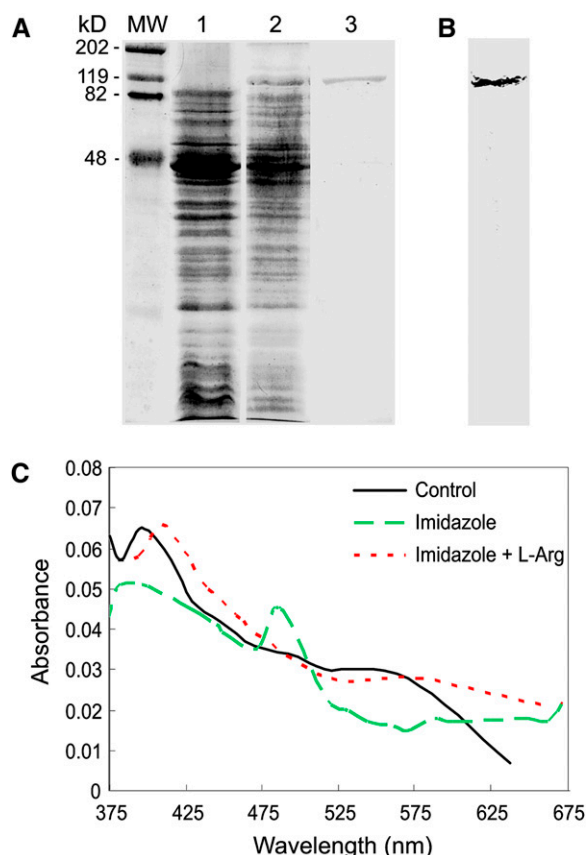


Figure 4. Purification and Spectral Characteristics of Recombinant NOS from *O. tauri* Expressed in *E. coli*.

(A) SDS-PAGE analysis of NOS during different steps of purification. Lane 1, cell extracts of *E. coli* transformed with the empty pET24b vector and induced with IPTG; lane 2, extracts of *E. coli* transformed with pET24b-OtNOS and induced with IPTG; lane 3, eluted fraction from 2',5'-ADP-agarose loaded with protein extracts from *E. coli* pET24b-OtNOS. MW, molecular weight standards.

(B) Immunoblot analysis of the eluted fraction from 2',5'-ADP-agarose using a specific anti-OtNOS antibody.

(C) Absolute absorbance spectra of recombinant NOS. Solid black line, unperturbed spectrum; dashed green line, after the addition of 1 mM imidazole; dotted red line, after the addition of 1 mM imidazole and 200 μ M L-Arg. Experiments were performed using 0.5 μ g purified NOS.

[See online article for color version of this figure.]

Similar results were obtained with the [3 H]L-citrulline method ($0.53 \pm 0.05 \mu$ M citrulline min^{-1}) in reactions containing L-Arg, the cofactor H₄B, CaM, and Ot NOS. L-citrulline formation was confirmed by thin layer chromatography (see Supplemental Figure 1 online). Activity assays indicate that recombinant *O. tauri* NOS is replete with FAD and FMN, since the enzyme retained its activity without adding these cofactors to the reaction (Table 1), as previously reported for recombinant bovine eNOS (Martasek et al., 1996). The K_m of *O. tauri* NOS for the substrate L-Arg estimated from the double reciprocal plot (see Supplemental Figure 2 online) using the oxyhemoglobin method was $12 \pm 5 \mu$ M. In absence of CaM, NOS retained up to 70% of

its activity (Table 1). NO and L-citrulline formation were undetectable in reactions that lacked H₄B and was inhibited by 80% by the inactive L-Arg analog, L-nitro arginine methylester (L-NAME) (Table 1). Results obtained from assays using a commercial recombinant iNOS from mouse were comparable to those obtained for *O. tauri* NOS either with the oxyhemoglobin method or [3 H]L-citrulline assay (Table 1).

The rate of NADPH oxidation by *O. tauri* NOS was also measured. A basal oxidation of NADPH in the absence of the substrate L-Arg ($0.42 \pm 0.2 \text{ min}^{-1}$) was subtracted in all measurements. A similar basal oxidation of NADPH has been reported for measurements of nNOS and eNOS activity (Heinzel et al., 1992; Martasek et al., 1996). In a reaction containing L-Arg and all cofactors, 0.5 μ M *O. tauri* NOS oxidized $1.36 \pm 0.18 \mu$ M NADPH min^{-1} . NADPH oxidation by *O. tauri* NOS was completely blocked in the absence of H₄B or by the addition of the inhibitor L-NAME.

Recombinant *O. tauri* NOS-Dependent NO Production in Bacteria

The ability of *E. coli* cell cultures transformed with *O. tauri* NOS to generate NO was assayed. The substrate L-Arg was added at the time of induction by isopropyl thiogalactoside (IPTG), and NO production was monitored over a 120-min period. *E. coli* transformed with the empty vector pET24b or the recombinant protein *O. tauri* NOS did not produce a significant amount of NO under basal conditions (Figures 5A and 5B). The addition of L-Arg to cells transformed with the empty vector triggered negligible NO production compared with the control. However, bacteria expressing recombinant *O. tauri* NOS produced up to 2.5-fold more NO than did control cells (Figures 5A and 5B). The inactive enantiomer D-Arg failed to trigger NO formation in both cultures (Figure 5B).

Gusarov and Nudler (2005) showed that NO confers cytoprotection to oxidative stress in bacteria. To investigate the tolerance of *O. tauri* NOS-transformed bacteria to oxidative stress, we analyzed the induction of cell death by exposure to H₂O₂. Figure 5C shows that, under resting conditions, the fold increase in cell death was 0.6 in NOS-transformed cells compared with those transformed with pET24b alone. H₂O₂ treatment induced an increase in cell death of 30% in the control strain and was 80% higher than in the H₂O₂-treated NOS-transformed cells (Figure 5C). The ratio of cell death in H₂O₂-treated versus untreated cells was similar in both pET24b and NOS-transformed cells, indicating that NOS protection of *E. coli* from cell death is H₂O₂ independent. As shown in Figure 5D, cells transformed with NOS had greater NO levels than cells transformed with the empty vector. Even though higher NO levels were measured in NOS-transformed bacteria, both strains accumulated NO when exposed to H₂O₂ (Figure 5D).

NO Production in *O. tauri* Cell Cultures

To analyze whether *O. tauri* produces NO in vivo, cell suspensions were incubated with the NO-specific fluorophore, 4-amino-5-methylamino-2',7'-difluorofluorescein diacetate (DAF-FM DA). NO generation was measured during the 60-min period following

Table 1. Activity of Purified Recombinant *O. tauri* NOS

Conditions	NOS	NO Formation (min ⁻¹)	%	Citrulline Formation (min ⁻¹)	%
Cofactors omitted					
None	<i>O. tauri</i> NOS	0.49 ± 0.03	100	0.53 ± 0.05	100
CaM	<i>O. tauri</i> NOS	0.35 ± 0.01	71	0.37 ± 0.01	69
H ₄ B	<i>O. tauri</i> NOS	<0.001	<1.0	<0.001	<1.0
Addition of inhibitor ^a					
L-NAME	<i>O. tauri</i> NOS	0.10 ± 0.10	20	<0.001	<1.0
Cofactors omitted					
None	iNOS	0.59 ± 0.13	120	0.41 ± 0.14	77

NO production was determined by the oxyhemoglobin method. Activity was measured for 3 min at 25°C in reaction containing 20 μM oxyhemoglobin, 5 mM DTT, 100 μM L-Arg, 1 mM NADPH, 10 mM CaCl₂, 10 μM CaM, 100 μM H₄B, 100 units/mL catalase, and 0.5 μM *O. tauri* NOS or commercial iNOS (Sigma-Aldrich). [³H]-citrulline formation was measured for 30 min in a reaction containing 1 μCi [³H] L-Arg, 50 μM unlabeled L-Arg, 100 μM NADPH, 10 μM FAD, 2 mM CaCl₂, 1 μg CaM, 100 μM H₄B, and 0.5 μM *O. tauri* NOS or commercial iNOS. L-NAME was used at concentration 100 μM. Activity assays were performed without adding FAD and FMN. The maximal activity was obtained without adding FAD and FMN, indicating that recombinant *O. tauri* NOS is replete with FAD and FMN as was previously described for other NOS recombinant activities (Martasek et al., 1996).

^aActivity assay in presence of all cofactors.

the addition of L-Arg. Figure 6A shows that, within the first 30 min, L-Arg promoted NO production in a dose-dependent manner (0.5 to 5 mM L-Arg), reaching maximum production at 5 mM L-Arg (8-fold induction). The NOS inhibitors L-NAME, G-monomethyl-L-arginine (L-NMMA), and NG-nitro-L-arginine (L-NNA) were used to confirm the source of NO production in L-Arg-treated *O. tauri* cells. Figure 6B shows that NOS inhibitors and the NO scavenger 2-(4-carboxyphenyl)-4,4,5,5-tetramethylimidazole-1-oxide decreased NO production. Furthermore, the CaM antagonist trifluoperazine dihydrochloride (TFP) caused a 30% reduction in NO production, and this result correlated with the activity of purified NOS protein in the absence of CaM (Table 1). Microscopy analysis showed that NO fluorescence (excitation 495 nm; emission 515 nm) increased significantly when cells were treated with 5 mM L-Arg compared with the untreated control (Figure 6C). *O. tauri* cells also displayed red fluorescence, which is attributed to chlorophyll autofluorescence (Figure 6C).

NOS activity in *O. tauri* cells depends on the phase of culture growth and on light irradiance conditions. Figure 7A shows that NO production was highest at the exponential growth phase and rapidly dropped at the start of the stationary growth phase. Shifting the cell culture from a light irradiance of 40 μmol m⁻² s⁻¹ to 100 μmol m⁻² s⁻¹ triggered an increase in NO production, both in the presence and absence of L-Arg (Figure 7B). Immunoblot analysis using anti-iNOS indicated that the addition of L-Arg did not increase the level of *O. tauri* NOS in *O. tauri* cell culture, whereas the shift from low to high irradiance induced the accumulation of NOS (Figure 7C). The specificity of anti-iNOS against *O. tauri* NOS was confirmed by immunoprecipitating *O. tauri* NOS with anti-OtNOS and then testing for the presence of *O. tauri* NOS with anti-iNOS (see Supplemental Figure 3 online).

The exposure of photosynthetic organisms to photoinhibitory intensities of light irradiance results in oxidative stress due to the imbalance between the light energy absorbed and the maximum energy that can be used in photosynthesis. NO production in *O. tauri* challenged by a 10× increase in irradiance (from 40 to 400 μmol m⁻² s⁻¹) was investigated. It has been reported that this large and sudden increase in light irradiance provokes reversible

photoinhibition (Six et al., 2009). Figure 7D shows that NO production was induced ~1.75-fold in photoinhibited *O. tauri* cell cultures challenged by 400 μmol m⁻² s⁻¹ compared with the control cells maintained at 40 μmol m⁻² s⁻¹. NO production returned to almost basal levels when the stressed culture was irradiated at 40 μmol m⁻² s⁻¹ for 18 h (Figure 7D).

DISCUSSION

NOS Is Present in Photosynthetic Organisms

In this work, we characterized a NOS from *O. tauri*, a green alga of class Prasinophyceae that branches near the base in the phylogenetic tree of photosynthetic organisms. The *O. tauri* NOS sequence contains the characteristic oxygenase and reductase domains joined by a CaM binding domain. *O. lucimarinus*, another species of the *Ostreococcus* genus, also contains a NOS gene, the expression of which was validated by EST analysis (Lanier et al., 2008). Whereas the *O. lucimarinus* NOS sequence has just one intron (Lanier et al., 2008), that of the predicted *O. tauri* NOS sequence (Derelle et al., 2006) contains a second micro-intron (41 nucleotides). It was not verified if this micro-intron is present in the *O. tauri* NOS gene or if it is predicted as a consequence of an error in the sequencing process. Thus, the recombinant *O. tauri* NOS sequence used for biochemical studies in this work may not be the same as the native *O. tauri* NOS sequence. The predicted micro-intron in *O. tauri* NOS sequence is located between the binding regions of FAD pyrophosphate and FAD isoalloxazine. Since it does not involve a domain that is critical for cofactor binding, it appears not to affect the activity of the recombinant *O. tauri* NOS protein.

Phylogenetic Analysis Reveals That *O. tauri* NOS Clusters with NOS from Cyanobacteria and Amoebozoa as an Outgroup of Metazoa NOS

The study of the phylogenetic relationship between *O. tauri* NOS and known NOS sequences suggests that *O. tauri* NOS is an

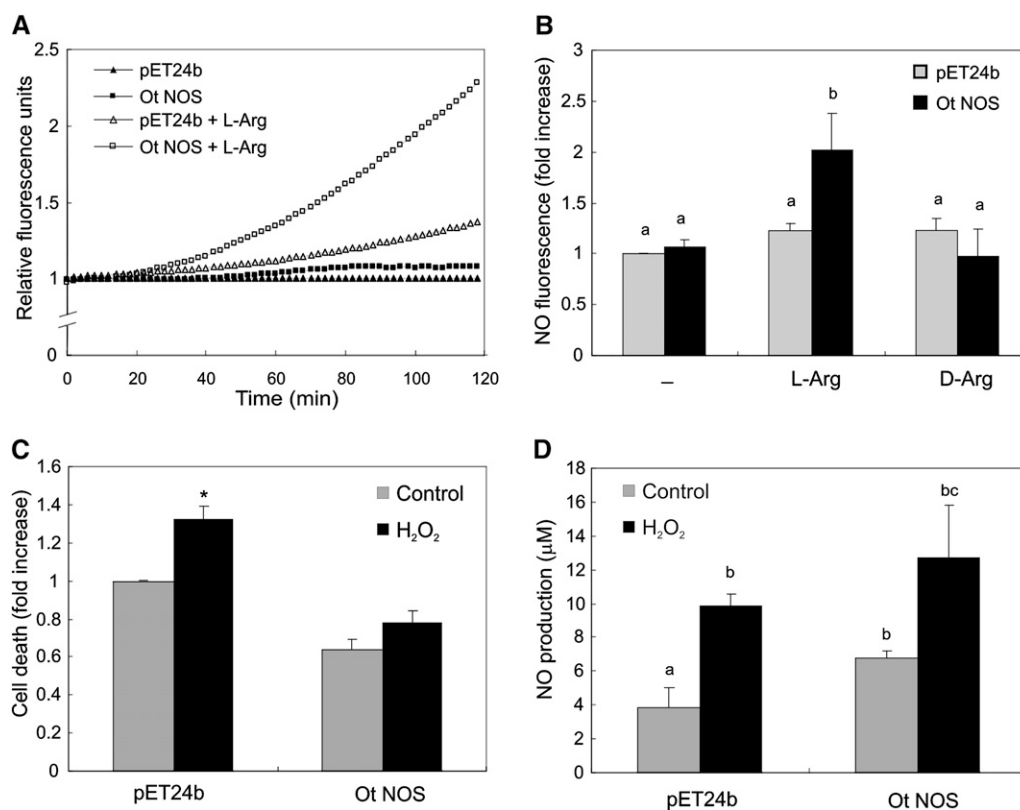


Figure 5. NO Production and Peroxide Sensitivity in *E. coli* Expressing Recombinant *O. tauri* NOS.

(A) *E. coli* culture was induced with IPTG in the presence or absence of 1 mM L-Arg. NO fluorescence was determined in a fluorometer using the DAF-FM DA probe. Data are expressed as fold increase of arbitrary units per min with respect to the control (*E. coli* transformed with the empty vector pET24b). A representative graph of three independent experiments is shown.

(B) IPTG-induced *E. coli* cultures (expressing *O. tauri* NOS or harboring an empty pET24b vector) were treated with 1 mM L-Arg or D-Arg. Fluorescence was determined in the presence of DAF-FM DA over a 2-h period. Data expressed as fold increase with respect to the control. Different letters indicate statistically significant differences (ANOVA, $P < 0.05$). Error bars denote SE ($n = 3$).

(C) *E. coli* cultures were treated with 30 mM H₂O₂ for 30 min in the presence of 1 mM L-Arg. Cell death was determined using the Sytox Green probe. Values are expressed as fold increase with respect to the control. The asterisk indicates statistically significant difference between the H₂O₂ treatment and the control (t test, $P < 0.05$). Error bars denote SE ($n = 5$).

(D) NO content measured with the Griess reagent. Different letters indicate a statistically significant difference (ANOVA, $P < 0.05$). Error bars denote SE ($n = 3$).

evolutionarily close relative of NOS from animals. *O. tauri* NOS appears in a well-supported cluster with *Synechococcus* PCC 7335 and *P. polycephalum*, a representative of Cyanobacteria and Amoebozoa, respectively. One interesting finding is that the NOS gene is only present in one out of the 13 *Synechococcus* genomes that have been completely sequenced. Evidence suggests that, in marine picocyanobacteria, the full complement of genes exists in a supragenome, since no single isolate contains the full complement of genes (Scanlan et al., 2009). The high levels of diversity of the gene complement and the efficiency of horizontal gene transfer (HGT) have been postulated to play major roles in the metagenome and population diversity of coastal *Synechococcus* (Palenik et al., 2009). *Synechococcus* PCC 7335 appears to be an unusual unicellular organism, since it is the only nonheterocystous N₂-fixing cyanobacterium currently assigned to this genus (Bergman et al., 1997). It will be interesting to study the role of NOS-dependent NO production in this strain.

A homolog of the *Synechococcus* PCC 7335 NOS gene is found in the fresh water bacterium *Spirosoma linguale* but not in other related organisms. Similarly, a homolog of *P. polycephalum* NOS (Messner et al., 2009) is not found in the completely sequenced genomes of closely related species, such as *Dicystostelium discoideum*. These findings could suggest that the NOS gene may be mobile within different unicellular organisms as a result of HGT. HGT is considered to be an important evolutionary force that modulates eukaryotic genomes (Keeling and Palmer, 2008). In *Ostreococcus*, two chromosomes (2 and 19) are different from the remaining 18 in terms of organization and C+G content. It has been suggested that the entire chromosome 19 may have been derived from an exogenous source by HGT (Derelle et al., 2006). Nevertheless, gene loss events cannot be discarded as a possible explanation for the available data.

Different structures of NOS genes are present in terrestrial and aquatic environments. However, there is currently not enough

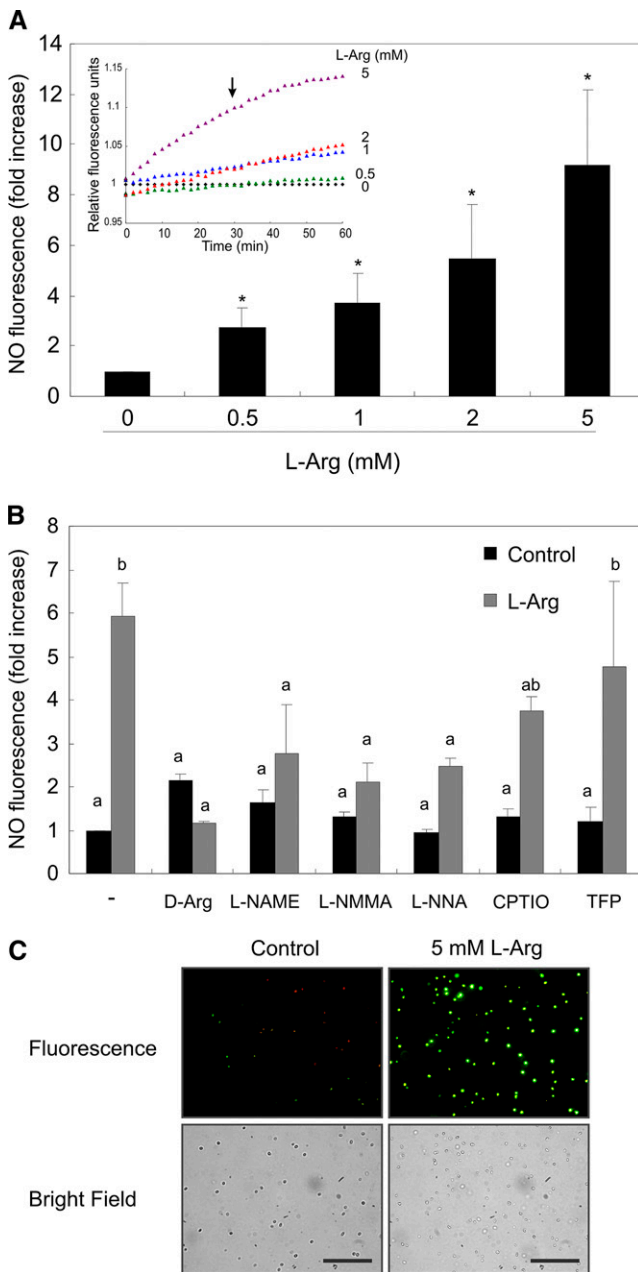


Figure 6. NO Generation by *O. tauri*.

(A) NO fluorescence emitted by *O. tauri* cells (grown at $100 \mu\text{mol m}^{-2} \text{s}^{-1}$ light irradiance) was determined using the probe DAF-FM DA in the presence of different concentrations of L-Arg. Data are expressed as fold increase (arbitrary units per min) with respect to the control. Inset: Representative graph of three independent experiments. Arrow indicates the point used for calculations of NO production. Asterisks indicate a statistically significant difference (*t* test, $P < 0.05$). Error bars denote SE ($n = 3$).

(B) NO fluorescence was determined in an *O. tauri* cell culture treated with 5 mM L-Arg in the presence and absence of the NOS inhibitors, L-NAME (10 mM), L-NMMA (10 mM), and L-NNA (10 mM), the specific NO scavenger 2-(4-carboxyphenyl)-4,4,5,5-tetramethylimidazoline-1-oxyl-3-oxide (CPTIO) (20 μM), or the CaM antagonist TFP (100 μM). Data are expressed as fold increase (arbitrary units per min) with respect to the

information to establish a correlation between habitats and the presence and structure of NOS genes in different organisms. It will be interesting to investigate the evolutionary forces that link ecological niches with the molecular evolution of NOS.

Recombinant *O. tauri* NOS Is an Active and Functional Enzyme

The recombinant *O. tauri* NOS produced in *E. coli* was a soluble and functional enzyme that exhibited a high level of enzyme activity, similar to that of macrophage iNOS from mouse (Table 1; Stuehr et al., 1991). The K_m value of recombinant *O. tauri* NOS for L-Arg is $12 \pm 5 \mu\text{M}$, which is within the range of previously characterized NOS enzymes (1 to 22 μM ; Bredt and Snyder, 1990; Stuehr et al., 1991; Roman et al., 1995; Gerber et al., 1997). We cannot state whether the enzyme is catalytically active as a monomer or dimer. A few studies indicate that the constitutive NOS in animals can be active as a monomer (Bredt and Snyder, 1990; Mayer et al., 1991), while macrophage iNOS is only active as a dimer (Stuehr et al., 1991). The presence of the four regions involved in the dimerization interface (Bird et al., 2002) supports the hypothesis that the active form of *O. tauri* NOS is a dimer. A dimer of the *O. tauri* NOS oxygenase domain was modeled and resembles that of human iNOS (see Supplemental Figure 4 online). The C-(x)₄-C zinc binding motif is strictly conserved across NOS sequences and is required for dimer stability (Hemmens et al., 2000). The zinc atom is tetrahedrally coordinated to two C residues from each NOS subunit. A C-(x)₃-C motif has thus far only been described in NOS proteins from *O. tauri* and *O. lucimarinus*. However, the zinc finger domain present in the GATA family of transcription factors is C-(x)₂-C (Aita et al., 2000), and the zinc finger domain of the cytochrome oxidase has a highly conserved C-(x)₃-C motif (Jaksch et al., 2001), indicating that the C-(x)₃-C motif present in *O. tauri* NOS could bind zinc. Moreover, the amino acids P and R are present within (x)₃, between the two C residues in the putative zinc binding domains [C-(x)₃-C] of NOS from *Ostreococcus* species and are conserved among most eNOS proteins described to date. Nevertheless, both the dimerization of *O. tauri* NOS subunits and the binding of zinc remain to be experimentally verified.

Macrophage iNOS binds CaM even at very low Ca^{2+} concentrations; thus, iNOS activity is Ca^{2+} -CaM independent (Mayer and Hemmens, 1997; Aoyagi et al., 2003). The results obtained from activity measurements and inhibitory assays in this work suggest that *O. tauri* NOS activity is mostly Ca^{2+} -CaM independent. The ACE segment that blocks electron flow in the absence of CaM is not present in *O. tauri* NOS or in any iNOS described but is present in nNOS and eNOS (Salerno et al., 1997).

The expression of recombinant *O. tauri* NOS in *E. coli* generates NO in vivo. It was demonstrated that the NO produced by bacterial NOS is required for maintaining a normal rate of cell

control. Different letters indicate a statistically significant difference (ANOVA, $P < 0.05$). Error bars denote SE ($n = 3$).

(C) *O. tauri* cells treated or not with 5 mM L-Arg for 20 min in the presence of DAF-FM DA. NO fluorescence was visualized using a fluorescence microscope. Bars = 50 μm .

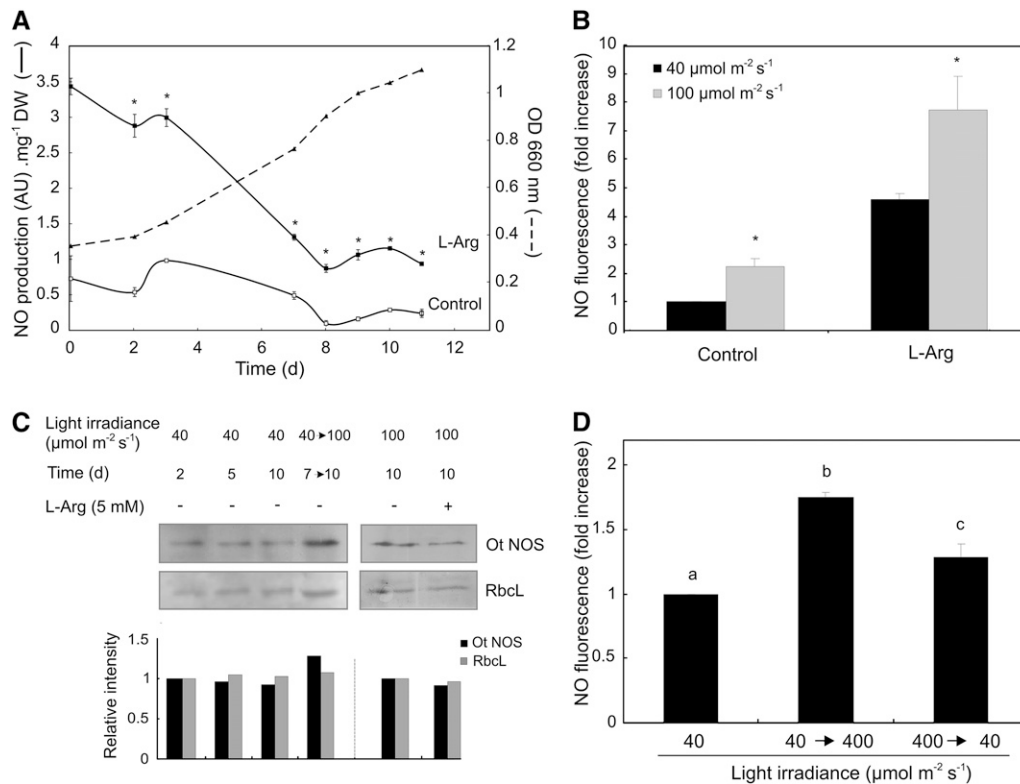


Figure 7. NO Generation Is Light Irradiance and Growth Phase Dependent.

(A) *O. tauri* cells were grown at 40 $\mu\text{mol m}^{-2} \text{s}^{-1}$ light irradiance. Culture growth was determined by measuring the OD at 660 nm. NO production was determined using DAF-FM DA with or without the addition of 5 mM L-Arg. Asterisks indicate a statistically significant difference (*t* test, $P < 0.05$). Error bars denote SE ($n = 3$). AU, arbitrary units; DW, dry weight.

(B) *O. tauri* cells grown at 40 $\mu\text{mol m}^{-2} \text{s}^{-1}$ of light irradiance for 10 d were transferred to 100 $\mu\text{mol m}^{-2} \text{s}^{-1}$ for 24 h. NO production was determined in the presence or absence of 5 mM L-Arg using DAF-FM DA. Data are expressed as fold increase (arbitrary units per min) with respect to the control. Asterisks indicate a statistically significant difference (*t* test, $P < 0.05$). Error bars denote SE ($n = 3$).

(C) Immunoblot analysis of NOS expression in *O. tauri* cultured for 2, 5, and 10 d at 40 $\mu\text{mol m}^{-2} \text{s}^{-1}$ light irradiance or 7 d at 40 $\mu\text{mol m}^{-2} \text{s}^{-1}$ and shift to 100 $\mu\text{mol m}^{-2} \text{s}^{-1}$ for another 3 d (7 → 10). In another experiment, cells were grown at 100 $\mu\text{mol m}^{-2} \text{s}^{-1}$ light irradiance for 10 d and treated with or without 5 mM L-Arg for 1 h. Ot NOS protein was detected with a commercial anti-iNOS antibody. The ribulose-1,5-bisphosphate carboxylase/oxygenase large subunit (RbcL) stained with Ponceau was included as a protein loading control. Relative quantification of Ot NOS and RbcL from blots using Image J software is shown in the bar graph.

(D) *O. tauri* cells grown at 40 $\mu\text{mol m}^{-2} \text{s}^{-1}$ were transferred to 400 $\mu\text{mol m}^{-2} \text{s}^{-1}$ for 1 h and then returned to 40 $\mu\text{mol m}^{-2} \text{s}^{-1}$ for 18 h. NO production was assayed using the fluorescent probe DAF-FM DA. Data are expressed as fold increase (arbitrary units per min) with respect to cells grown at 40 $\mu\text{mol m}^{-2} \text{s}^{-1}$. Different letters indicate a statistically significant difference (ANOVA, $P < 0.05$). Error bars denote SE ($n = 3$).

growth at the beginning of the stationary phase (Gusarov et al., 2008). The addition of H_2O_2 induced an increase in NO production in *E. coli* transformed with the empty vector; however, this basal NO increase failed to protect the cells against the harmful effects of H_2O_2 . Since *E. coli* lacks NOS, the evolution of NO following H_2O_2 treatment could be due to the ability of certain nitrite reductases to reduce nitrite to NO. NO production by *E. coli* cultures was reported elsewhere (Hutchings et al., 2000; Corker and Poole, 2003). Moreover, H_2O_2 is able to generate NO nonenzymatically from L- or D-Arg (Nagase et al., 1997; Gotte et al., 2002). *E. coli* has a complex set of responses to H_2O_2 and O^{-2} that involves ~80 inducible proteins and is regulated by the redox-sensitive transcriptional regulator SoxR (Greenberg et al., 1990; Liochev et al., 1994). Interestingly, the *E. coli* SoxR-regulated redox stress response was found to be induced by

NO and to confer bacterial resistance to activated murine macrophages (Nunoshiba et al., 1993).

NOS Is Expressed in *O. tauri* and Is Functionally Influenced by Light Irradiance and Growth Phase of the Microalga

O. tauri cells have a high level of NOS-dependent NO production during the exponential growth phase of the culture. This NO production can be augmented by the exogenous addition of L-Arg. Several studies demonstrate that L-Arg availability is an important factor in NO production (El-Gayar et al., 2003; Lee et al., 2003). Endogenous L-Arg availability may be regulated by (1) increasing the de novo synthesis of L-Arg, (2) increasing L-Arg transport across the cell membrane, and (3) reducing L-Arg breakdown by arginase (Hallemeesch et al., 2002; Flores

et al., 2008). Several reports confirm that microalgae excrete free amino acids into the media (Martin-Jézéquel et al., 1988; Penteado et al., 2009). Our results demonstrate that the increase in external L-Arg concentration can significantly enhance NOS-dependent NO production in *Ostreococcus*. This may be related to the development and ecology of algal blooms in picophytoplankton (Mayali and Azam, 2004; Tillmann, 2004).

NO can participate at different levels during algal bloom successions. Expression of the death-specific protein in the marine diatom *Skeletonema costatum* is induced by NO, high irradiance, and photoinhibitory compounds (Chung et al., 2008). Vardi et al. (2006) have shown that, in marine diatoms, reactive aldehydes promote the production of large amounts of NO through a NOS-like activity and induce cell death. In a more recent work, Vardi et al. (2008) also demonstrated that a high level of NO production associated with a GTP binding protein was responsible for reduced growth and impaired photosynthetic efficiency in the marine diatom *Phaeodactylum tricoratum*. Thus, several lines of evidence indicate that augmented NO generation is closely related to the regulation of algal bloom evolution. Hence, L-Arg-dependent NO production during the life cycle of *Ostreococcus* points to the potential impact of amino acid excretion on both the algal bloom and the marine nitrogen (N) cycle. N is the only essential element whose concentration in seawater is controlled by biological activity (Morel, 2008).

Marine photosynthetic organisms confront environmental changes, such as changes in light and temperature, during the day. Irradiation of a photosynthetic organism with photoinhibitory light intensities provokes the photoinactivation of photosystem II (PSII) and generates an oxidative stress response that can damage biomolecules. To counter photoinactivation, *O. tauri* removes the photoinactivated D1 protein from PSII and replaces it through de novo synthesis and reassembly of PSII (Six et al., 2009). NO is a potent antioxidant molecule that was shown to protect lipids, proteins (including D1 protein), and nucleic acids from the photooxidative damage generated by bipyridinium herbicides in higher plants (Beligni and Lamattina, 2002). The induction of NOS activity in *O. tauri* upon exposure to photoinhibitory light intensities may reduce oxidative damage and promote the repair of this damage.

This report provides compelling evidence that an active NOS functions in a photosynthetic organism belonging to the plant kingdom and that this enzyme contains the main characteristics of the NOS enzymes present in animals.

METHODS

Materials

L-Arg, 2'-5-ADP-agarose, CaM, H₄B, TFP, hemoglobin, anti-iNOS antibody from mouse, and recombinant mouse iNOS (16.8 units/mg protein) were purchased from Sigma-Aldrich. The NOS inhibitors L-NAME, L-NMMA, and L-NNA were obtained from Calbiochem. The DNA clone for the coding sequence of the NOS gene from *Ostreococcus tauri* (Ot NOS) and the polyclonal anti-OtNOS antibody were acquired from Genscript. Restriction enzymes, Bacto-yeast extract, IPTG, and *Escherichia coli* DH5 α cells were purchased from Life Technologies. *BL21* (DE3) pLys cells and pET24b were from Novagen. *O. tauri* (strain OTTH 0595)

was purchased from the Roscoff Culture Collection (Station Biologique, Roscoff, France).

Homology Modeling

Fold assignment was performed using FFAS03 (Jaroszewski et al., 2005) and HHPred (Söding et al., 2005). Structural models were built with the program MODELER v 9.5 (Sali and Blundell, 1993) using ClustalX- and FFAS03-derived alignments with explicit consideration for the presence of ligands and the oligomeric state. The template was selected using FFAS03 and corresponds to the crystal structure of the NOSoxy region of *Bos taurus* eNOS and of the NOSred region of nNOS from *Rattus norvegicus*. The model was validated using PROSA II software (Wiederstein and Sippl, 2007), and the figures were drawn using Web Lab ViewerLite 3.20 software (Molecular Simulations). Structural superposition of *O. tauri* NOS and *B. taurus* eNOS was performed with the program SuperPose (Maiti et al., 2004). *O. tauri* NOS and human NOS were aligned using ClustalX software (version 1.81; Thompson et al., 1997) and edited with GeneDoc software (version 2.5.010).

Sequence Data and Phylogenetic Analysis

Protein sequences with similarity to *O. tauri* NOS (E-value < 1.10⁻¹¹⁰) were retrieved using BLAST and the nonredundant database from GenBank (see Supplemental Table 1 online). CDHIT software (Huang et al., 2010) was used to remove all sequences sharing >90% identity. The sequences were aligned with ClustalX and edited with GeneDoc software (see Supplemental Data Set 1 online). Domain organization was analyzed using InterPro database (Hunter et al., 2009) and PFAM (Finn et al., 2008). Maximum likelihood phylogenetic analyses were performed with PHYML (Guindon and Gascuel, 2003). The best evolutionary model for the phylogenetic inference was estimated using ModelTest (Posada and Crandall, 1998). Nonparametric bootstrapping (1000 replicates) was used to assess tree branching support. The program iTOL (Letunic and Bork, 2007) was used to display phylogenetic trees (<http://itol.embl.de/>).

DNA Manipulation

The *O. tauri* NOS coding DNA sequence was synthesized, sequenced, and cloned into pUC57 using *Xba*I and *Xho*I enzymes. pUC57-OtNOS was digested with *Bam*HI and *Sac*I to yield a fragment of 3258 bp. The product was purified and subcloned into pET24b. The ligation product was used to transform *E. coli* DH5 α . Colonies were screened by PCR using the following primers: forward, 5'-GCTGGGCGCCGAAAA-GAC-3', and reverse, 5'-GCGCCGGCCGAACTCAAC-3'. The expected product length was 2031 bp. pET24b-OtNOS was used to transform *BL21* protease-deficient *E. coli* via electroporation. This strain is deficient in the proteases ompT and lon, resulting in a suitable host for optimal recombinant expression (Sørensen and Mortensen, 2005).

Protein Expression and Purification

Fernbach flasks containing 1 liter of modified Terrific Broth (20 g of yeast extract, 10 g of bactotryptone, 2.65 g of KH₂PO₄, 4.33 g of Na₂HPO₄, and 4 mL of glycerol) and kanamycin (50 μ g/mL) were inoculated with 1 mL of culture and shaken at 190 rpm at 30°C. Recombinant protein expression was induced at OD₆₀₀ = 0.6 by the addition of 0.5 mM IPTG. The heme and flavin precursors 8-aminolevulinic acid and riboflavin were added to final concentrations of 450 and 3 μ M, respectively.

Cells were harvested after 40 h of induction and were resuspended in 30 mL of buffer (100 mM Tris-HCl, pH 7.4, 1 mM EDTA, 1 mM DTT, 10% [v/v] glycerol, 1 mM PMSF, 5 μ g/mL leupeptin, and 5 μ g/mL pepstatin) per liter of initial culture and lysed by pulsed sonication (six cycles of 20 s). Cell debris were removed by centrifugation, and the supernatant was

applied to a 2',5'-ADP-agarose 4B column (1 mL) equilibrated in buffer B (50 mM Tris-HCl, pH 7.4, 0.1 mM EDTA, 0.1 mM DTT, 10% glycerol, and 100 mM NaCl). The column was extensively washed with 10 column volumes of buffer B and finally with buffer B and 500 mM NaCl. The protein was eluted with buffer B, 500 mM NaCl, and 25 mM 2'-AMP.

Determination of NOS Activity

NO synthesis was assayed using two methods: (1) oxyhemoglobin and (2) [³H]L-citrulline formation. The oxyhemoglobin method was performed as described by Ghafourifar et al. (2005). Hemoglobin was completely reduced to oxyhemoglobin with sodium dithionite. The concentration of oxyhemoglobin in the solution was determined using a molar extinction coefficient of 131 mM⁻¹ cm⁻¹ at 415 nm. A 500-μL reaction containing 20 μM oxyhemoglobin, 7.5 mM HEPES-NaOH, pH 7.5, 5 mM DTT, 100 μM L-Arg, 1 mM NADPH, 10 mM CaCl₂, 10 μM CaM, 100 μM H₄B, and 100 units/mL catalase was prepared. The reaction was initiated by the addition of 0.5 μM purified *O. tauri* NOS protein. The NO-dependent conversion of oxyhemoglobin to methemoglobin was monitored on a spectrophotometer (Ultrospec 1100 pro; Amersham Biosciences) by scanning between 380 and 450 nm. An extinction coefficient of 100 mM⁻¹ cm⁻¹ between the peak at 401 nm and the valley at 420 nm was used to quantify NO production. Citrulline formation was determined as previously described (Bredt and Snyder, 1990). Enzymatic reactions were conducted at 25°C in 50 mM Tris-HCl, pH 7.4, containing 50 μM L-Arg, 1 μCi [³H]Arg monohydrochloride (40 to 70 Ci/mmol; Perkin-Elmer), 100 μM NADPH, 10 μM FAD, 2 mM CaCl₂, 1 μg CaM, and 100 μM H₄B in a volume of 40 μL. Enzymatic reactions were initiated by adding 0.5 μM NOS and terminated after 30 min by the addition of 400 μL of ice-cold 20 mM sodium acetate, pH 5.5, containing 1 mM L-citrulline, 2 mM EDTA, and 0.2 mM EGTA (stop buffer). Samples were applied to columns containing 1 mL of Dowex AG50W-X8, Na⁺ form (Bio-Rad; 100 to 200 mesh), preequilibrated with stop buffer. L-citrulline was eluted with 2 mL of distilled water. Aliquots of 0.5 mL of eluate were dissolved in 10 mL of scintillation liquid, and radioactivity was measured in a Beckman LS 3801 liquid scintillation system. The formation of L-citrulline was verified by thin layer chromatography.

NADPH oxidation was measured in a 500-μL volume containing 0.5 μM *O. tauri* NOS, 50 mM Tris-HCl, pH 7.6, 5 mM DTT, 100 μM L-Arg, 1 mM NADPH, 10 mM CaCl₂, 10 μM CaM, 10 μM H₄B, and 100 units/mL catalase. The rate of decrease in absorbance at 340 nm was monitored for 10 min at 25°C using a spectrophotometer. An extinction coefficient of 6.22 mM⁻¹ cm⁻¹ at 340 nm was used to calculate NADPH oxidation.

NO Production in Cultures

O. tauri cultures were grown in Erlenmeyer flasks containing K medium (Keller et al., 1987) at 20 ± 1°C under a 12 h:12 h (light:dark) photoperiod. Light experiments were conducted over irradiances ranging from 40 to 400 μmol m⁻² s⁻¹. NO content in the *E. coli* or *O. tauri* cultures was quantified using the NO-sensitive fluorescence probe DAF-FM DA (Invitrogen). DAF-FM DA (10 μM) was added to the culture medium 20 min before measurement. NO production was initiated by the addition of the substrate L-Arg. NO fluorescence intensity (excitation 495 nm; emission 515 nm) was measured using a fluorescence plate reader (Fluoroskan Ascent; Thermo Electron) or visualized under an inverted fluorescence microscope (Nikon Eclipse TI). NO formation in *E. coli* was also measured using the Griess reagent for nitrate measurement as described by Xu et al. (2000).

Cell Death Analysis

E. coli cultures were treated with 30 mM H₂O₂ for 30 min. Cells were stained with 2 μM of the membrane-impermeable dye SYTOX (Molecular

Probes) for 10 min in the dark at room temperature. Cells were washed with 1.5 volumes of fresh medium. Fluorescence intensity (excitation 480 nm; emission 525 nm) was measured using a fluorescence plate reader (Fluoroskan Ascent).

Statistical Analysis

Results are expressed as mean ± SE. Statistical analysis was performed employing SigmaStat statistical software (Jandel Scientific) using analysis of variance (ANOVA) for multiple comparison analyses and the *t* test for pairwise comparisons.

Accession Numbers

Sequence data from this article can be found in the GenBank/EMBL database under the following accession numbers: *O. tauri* NOS (CAL57731), eNOS (NP_000594), nNOS (NP_000611), iNOS (AAI30284), and *Spirosoma linguale* NOS (YP_003391026). The accession numbers for the amino acid sequences used in the phylogenetic analysis can be found in Supplemental Table 1 online. The crystal structures from this article can be found in the Protein Data Bank (www.rcsb.org) under the following codes: *R. norvegicus* nNOSred (1tl1) and *B. taurus* eNOSoxy (1fop).

Author Contributions

Experiments were designed by N.F., N.C.-A., G.P., G.C., G.S., and L.L. and conducted by N.F., G.C., and N.C.-A. Bioinformatic analyses were conducted by G.P., N.C.-A., N.F., and L.L. The manuscript was prepared and written by N.F., N.C.-A., and L.L. The design, supervision, and direction of the project were performed by L.L.

Supplemental Data

The following materials are available in the online version of this article.

Supplemental Figure 1. Detection of L-Citrulline as a Product of *O. tauri* NOS Enzymatic Activity.

Supplemental Figure 2. Double Reciprocal Lineweaver-Burk Plot of *O. tauri* NOS Activity versus L-Arg Concentration.

Supplemental Figure 3. Immunoprecipitation of *O. tauri* NOS Protein Using Anti-OtNOS Antibody.

Supplemental Figure 4. Tertiary Topology of *O. tauri* NOS Oxygenase Dimer.

Supplemental Table 1. Full Name and GI Number of All NOS Sequences Retrieved with BLAST and the Nonredundant Database from GenBank.

Supplemental Data Set 1. Alignment of NOS Proteins Used to Build the Phylogenetic Tree Presented in Figure 3.

ACKNOWLEDGMENTS

We thank E. Zabaleta for providing *E. coli* B12 cells and R. De Castro for providing pET24b. This research was supported by Agencia Nacional de Promoción Científica y Tecnológica (PICTs 38078/05 and 1-14457/03 to L.L.), Consejo Nacional de Investigaciones Científicas y Técnicas (CONICET; PIP 0898/98 to L.L.), and institutional grants from Universidad Nacional de Mar del Plata, Argentina. G.P., G.L., and L.L. are members of the research staff, and N.F. and N.C.-A. are postgraduate fellows from CONICET, Argentina.

Received December 15, 2009; revised September 17, 2010; accepted November 9, 2010; published November 30, 2010.

REFERENCES

- Adoutte, A., Balavoine, G., Lartillot, N., Lespinet, O., Prud'homme, B., and de Rosa, R. (2000). The new animal phylogeny: Reliability and implications. *Proc. Natl. Acad. Sci. USA* **97**: 4453–4456.
- Aita, V.M., Ahmad, W., Panteleyev, A.A., Kozłowska, U., Kozłowska, A., Gilliam, T.C., Jabłonska, S., and Christiano, A.M. (2000). A novel missense mutation (C622G) in the zinc-finger domain of the human hairless gene associated with congenital atrichia with papular lesions. *Exp. Dermatol.* **9**: 157–162.
- Alderton, W.K., Cooper, C.E., and Knowles, R.G. (2001). Nitric oxide synthases: Structure, function and inhibition. *Biochem. J.* **357**: 593–615.
- Aoyagi, M., Arvai, A.S., Tainer, J.A., and Getzoff, E.D. (2003). Structural basis for endothelial nitric oxide synthase binding to calmodulin. *EMBO J.* **22**: 766–775.
- Barroso, J.B., Corpas, F.J., Carreras, A., Sandalio, L.M., Valderrama, R., Palma, J.M., Lupiáñez, J.A., and del Río, L.A. (1999). Localization of nitric-oxide synthase in plant peroxisomes. *J. Biol. Chem.* **274**: 36729–36733.
- Beligni, M.V., and Lamattina, L. (2002). Nitric oxide interferes with plant photo-oxidative stress by detoxifying reactive oxygen species. *Plant Cell Environ.* **25**: 737–748.
- Bergman, B., Gallon, J.R., Rai, A.N., and Stal, L.J. (1997). N₂ Fixation by non-heterocystous cyanobacteria. *FEMS Microbiol. Rev.* **19**: 139–185.
- Bird, L.E., Ren, J., Zhang, J., Foxwell, N., Hawkins, A.R., Charles, I. G., and Stammers, D.K. (2002). Crystal structure of SANOS, a bacterial nitric oxide synthase oxygenase protein from *Staphylococcus aureus*. *Structure* **10**: 1687–1696.
- Bredt, D.S., and Snyder, S.H. (1990). Isolation of nitric oxide synthetase, a calmodulin-requiring enzyme. *Proc. Natl. Acad. Sci. USA* **87**: 682–685.
- Bright, J., Desikan, R., Hancock, J.T., Weir, I.S., and Neill, S.J. (2006). ABA-induced NO generation and stomatal closure in Arabidopsis are dependent on H₂O₂ synthesis. *Plant J.* **45**: 113–122.
- Caro, A., and Puntarulo, S. (1999). Nitric oxide generation by soybean embryonic axes. Possible effect on mitochondrial function. *Free Radic. Res.* **31** (suppl.): S205–S212.
- Chung, C.C., Hwang, S.-P.L., and Chang, J. (2008). Nitric oxide as a signaling factor to upregulate the death-specific protein in a marine diatom, *Skeletonema costatum*, during blockage of electron flow in photosynthesis. *Appl. Environ. Microbiol.* **74**: 6521–6527.
- Corker, H., and Poole, R.K. (2003). Nitric oxide formation by *Escherichia coli*. Dependence on nitrite reductase, the NO-sensing regulator Fnr, and flavohemoglobin Hmp. *J. Biol. Chem.* **278**: 31584–31592.
- Corpas, F.J., Palma, J.M., del Río, L.A., and Barroso, J.B. (2009). Evidence supporting the existence of L-arginine-dependent nitric oxide synthase activity in plants. *New Phytol.* **184**: 9–14.
- Crane, B.R., Sudhamsu, J., and Patel, B.A. (2010). Bacterial nitric oxide synthases. *Annu. Rev. Biochem.* **79**: 445–470.
- Cueto, M., Hernández-Perera, O., Martín, R., Bentura, M.L., Rodrigo, J., Lamas, S., and Golvano, M.P. (1996). Presence of nitric oxide synthase activity in roots and nodules of *Lupinus albus*. *FEBS Lett.* **398**: 159–164.
- Derelle, E., et al. (2006). Genome analysis of the smallest free-living eukaryote *Ostreococcus tauri* unveils many unique features. *Proc. Natl. Acad. Sci. USA* **103**: 11647–11652.
- Díez, B., Pedrós-Alió, C., and Massana, R. (2001). Study of genetic diversity of eukaryotic picoplankton in different oceanic regions by small-subunit rRNA gene cloning and sequencing. *Appl. Environ. Microbiol.* **67**: 2932–2941.
- El-Gayar, S., Thüring-Nahler, H., Pfeilschifter, J., Röllinghoff, M., and Bogdan, C. (2003). Translational control of inducible nitric oxide synthase by IL-13 and arginine availability in inflammatory macrophages. *J. Immunol.* **171**: 4561–4568.
- Finn, R.D., Tate, J., Mistry, J., Coghill, P.C., Sammut, S.J., Hotz, H.R., Ceric, G., Forslund, K., Eddy, S.R., Sonnhammer, E.L., and Bateman, A. (2008). The Pfam protein families database. *Nucleic Acids Res.* **36** (Database issue): D281–D288.
- Flores, T., Todd, C.D., Tovar-Mendez, A., Dhanoa, P.K., Correa-Aragunde, N., Hoyos, M.E., Brownfield, D.M., Mullen, R.T., Lamattina, L., and Polacco, J.C. (2008). Arginase-negative mutants of Arabidopsis exhibit increased nitric oxide signaling in root development. *Plant Physiol.* **147**: 1936–1946.
- Gas, E., Flores-Pérez, U., Sauret-Güeto, S., and Rodríguez-Concepción, M. (2009). Hunting for plant nitric oxide synthase provides new evidence of a central role for plastids in nitric oxide metabolism. *Plant Cell* **21**: 18–23.
- Gerber, N.C., Nishida, C.R., and Ortiz de Montellano, P.R. (1997). Characterization of human liver inducible nitric oxide synthase expressed in *Escherichia coli*. *Arch. Biochem. Biophys.* **343**: 249–253.
- Ghafourifar, P., Asbury, M.L., Joshi, S.S., and Kincaid, E.D. (2005). Determination of mitochondrial nitric oxide synthase activity. *Methods Enzymol.* **396**: 424–444.
- Gorren, A.C.F., and Mayer, B. (2007). Nitric-oxide synthase: A cytochrome P450 family foster child. *Biochim. Biophys. Acta* **1770**: 432–445.
- Gotte, G., Amelio, E., Russo, S., Marlinghaus, E., Musci, G., and Suzuki, H. (2002). Short-time non-enzymatic nitric oxide synthesis from L-arginine and hydrogen peroxide induced by shock waves treatment. *FEBS Lett.* **520**: 153–155.
- Greenberg, J.T., Monach, P., Chou, J.H., Josephy, P.D., and Dimple, B. (1990). Positive control of a global antioxidant defense regulon activated by superoxide-generating agents in *Escherichia coli*. *Proc. Natl. Acad. Sci. USA* **87**: 6181–6185.
- Griffith, O.W., and Stuehr, D.J. (1995). Nitric oxide synthases: Properties and catalytic mechanism. *Annu. Rev. Physiol.* **57**: 707–736.
- Guindon, S., and Gascuel, O. (2003). A simple, fast, and accurate algorithm to estimate large phylogenies by maximum likelihood. *Syst. Biol.* **52**: 696–704.
- Gusarov, I., and Nudler, E. (2005). NO-mediated cytoprotection: Instant adaptation to oxidative stress in bacteria. *Proc. Natl. Acad. Sci. USA* **102**: 13855–13860.
- Gusarov, I., Starodubtseva, M., Wang, Z.Q., McQuade, L., Lippard, S.J., Stuehr, D.J., and Nudler, E. (2008). Bacterial nitric-oxide synthases operate without a dedicated redox partner. *J. Biol. Chem.* **283**: 13140–13147.
- Hallemeesch, M.M., Lamers, W.H., and Deutz, N.E. (2002). Reduced arginine availability and nitric oxide production. *Clin. Nutr.* **21**: 273–279.
- Heinzel, B., John, M., Klatt, P., Böhme, E., and Mayer, B. (1992). Ca²⁺/calmodulin-dependent formation of hydrogen peroxide by brain nitric oxide synthase. *Biochem. J.* **281**: 627–630.
- Hemmens, B., Goessler, W., Schmidt, K., and Mayer, B. (2000). Role of bound zinc in dimer stabilization but not enzyme activity of neuronal nitric-oxide synthase. *J. Biol. Chem.* **275**: 35786–35791.
- Hutchings, M.I., Shearer, N., Wastell, S., van Spanning, R.J.M., and Spiro, S. (2000). Heterologous NNR-mediated nitric oxide signaling in *Escherichia coli*. *J. Bacteriol.* **182**: 6434–6439.
- Huang, Y., Niu, B., Gao, Y., Fu, L., and Li, W. (2010). CD-HIT Suite: A web server for clustering and comparing biological sequences. *Bioinformatics* **26**: 680–682.
- Hunter, S., et al. (2009). InterPro: The integrative protein signature database. *Nucleic Acids Res.* **37** (Database issue): D211–D215.

- Jaksch, M., et al.** (2001). Cytochrome c oxidase deficiency due to mutations in SCO2, encoding a mitochondrial copper-binding protein, is rescued by copper in human myoblasts. *Hum. Mol. Genet.* **10**: 3025–3035.
- Jaroszewski, L., Rychlewski, L., Li, Z., Li, W., and Godzik, A.** (2005). FFAS03: a server for profile–profile sequence alignments. *Nucleic Acids Res.* **33** (Web Server issue): W284–W288.
- Keeling, P.J., and Palmer, J.D.** (2008). Horizontal gene transfer in eukaryotic evolution. *Nat. Rev. Genet.* **9**: 605–618.
- Keller, M.D., Selvin, R.C., Claus, W., and Guillard, R.R.L.** (1987). Media for the culture of oceanic ultraphytoplankton. *J. Phycol.* **23**: 633–638.
- Knudsen, G.M., Nishida, C.R., Mooney, S.D., and Ortiz de Montellano, P.R.** (2003). Nitric-oxide synthase (NOS) reductase domain models suggest a new control element in endothelial NOS that attenuates calmodulin-dependent activity. *J. Biol. Chem.* **278**: 31814–31824.
- Lanier, W., Moustafa, A., Bhattacharya, D., and Comeron, J.M.** (2008). EST analysis of *Ostreococcus lucimarinus*, the most compact eukaryotic genome, shows an excess of introns in highly expressed genes. *PLoS ONE* **3**: e2171.
- Lee, J., Ryu, H., Ferrante, R.J., Morris, S.M., Jr., and Ratan, R.R.** (2003). Translational control of inducible nitric oxide synthase expression by arginine can explain the arginine paradox. *Proc. Natl. Acad. Sci. USA* **100**: 4843–4848.
- Letunic, I., and Bork, P.** (2007). Interactive Tree Of Life (iTOL): An online tool for phylogenetic tree display and annotation. *Bioinformatics* **23**: 127–128.
- Liochev, S.I., Hausladen, A., Beyer, W.F., Jr., and Fridovich, I.** (1994). NADPH: Ferredoxin oxidoreductase acts as a paraquat diaphorase and is a member of the soxRS regulon. *Proc. Natl. Acad. Sci. USA* **91**: 1328–1331.
- Lowe, P.N., Smith, D., Stammers, D.K., Riveros-Moreno, V., Moncada, S., Charles, I., and Boyhan, A.** (1996). Identification of the domains of neuronal nitric oxide synthase by limited proteolysis. *Biochem. J.* **314**: 55–62.
- Maiti, R., Van Domselaar, G.H., Zhang, H., and Wishart, D.S.** (2004). SuperPose: A simple server for sophisticated structural superposition. *Nucleic Acids Res.* **32** (Web Server issue): W590–W594.
- Martasek, P., Liu, Q., Liu, J., Roman, L.J., Gross, S.S., Sessa, W.C., and Masters, B.S.** (1996). Characterization of bovine endothelial nitric oxide synthase expressed in *E. coli*. *Biochem. Biophys. Res. Commun.* **219**: 359–365.
- Martin-Jézéquel, V., Poulet, S.A., Harris, R.P., Moal, J., and Samain, J.F.** (1988). Interspecific and intraspecific composition and variation of free amino acids in marine phytoplankton. *Mar. Ecol.* **44**: 303–313.
- Mayali, X., and Azam, F.** (2004). Algicidal bacteria in the sea and their impact on algal blooms. *J. Eukaryot. Microbiol.* **51**: 139–144.
- Mayer, B., and Hemmens, B.** (1997). Biosynthesis and action of nitric oxide in mammalian cells. *Trends Biochem. Sci.* **22**: 477–481.
- Mayer, B., John, M., Heinzl, B., Werner, E.R., Wachter, H., Schultz, G., and Böhme, E.** (1991). Brain nitric oxide synthase is a biopterin- and flavin-containing multi-functional oxido-reductase. *FEBS Lett.* **288**: 187–191.
- Messner, S., Leitner, S., Bommassar, C., Golderer, G., Gröbner, P., Werner, E.R., and Werner-Felmayer, G.** (2009). Physarum nitric oxide synthases: Genomic structures and enzymology of recombinant proteins. *Biochem. J.* **418**: 691–700.
- Morel, F.M.** (2008). The co-evolution of phytoplankton and trace element cycles in the oceans. *Geobiology* **6**: 318–324.
- Nagase, S., Takemura, K., Ueda, A., Hirayama, A., Aoyagi, K., Kondoh, M., and Koyama, A.** (1997). A novel nonenzymatic pathway for the generation of nitric oxide by the reaction of hydrogen peroxide and D- or L-arginine. *Biochem. Biophys. Res. Commun.* **233**: 150–153.
- Nunoshiba, T., deRojas-Walker, T., Wishnok, J.S., Tannenbaum, S.R., and Demple, B.** (1993). Activation by nitric oxide of an oxidative-stress response that defends *Escherichia coli* against activated macrophages. *Proc. Natl. Acad. Sci. USA* **90**: 9993–9997.
- Palenik, B., Ren, Q., Tai, V., and Paulsen, I.T.** (2009). Coastal Synechococcus metagenome reveals major roles for horizontal gene transfer and plasmids in population diversity. *Environ. Microbiol.* **11**: 349–359.
- Penteado, J.C., Rigobello-Masini, M., Liria, C.W., Miranda, M.T., and Masini, J.C.** (2009). Fluorimetric determination of intra- and extracellular free amino acids in the microalgae *Tetraselmis gracilis* (Prasinophyceae) using monolithic column in reversed phase mode. *J. Sep. Sci.* **32**: 2827–2834.
- Posada, D., and Crandall, K.A.** (1998). MODELTEST: Testing the model of DNA substitution. *Bioinformatics* **14**: 817–818.
- Rhoads, A.R., and Friedberg, F.** (1997). Sequence motifs for calmodulin recognition. *FASEB J.* **11**: 331–340.
- Ribeiro, E.A., Jr., Cunha, F.Q., Tamashiro, W.M., and Martins, I.S.** (1999). Growth phase-dependent subcellular localization of nitric oxide synthase in maize cells. *FEBS Lett.* **445**: 283–286.
- Roman, L.J., Sheta, E.A., Martasek, P., Gross, S.S., Liu, Q., and Masters, B.S.** (1995). High-level expression of functional rat neuronal nitric oxide synthase in *Escherichia coli*. *Proc. Natl. Acad. Sci. USA* **92**: 8428–8432.
- Rousseau, D.L., Li, D., Couture, M., and Yeh, S.R.** (2005). Ligand-protein interactions in nitric oxide synthase. *J. Inorg. Biochem.* **99**: 306–323.
- Salerno, J.C., et al.** (1997). An autoinhibitory control element defines calcium-regulated isoforms of nitric oxide synthase. *J. Biol. Chem.* **272**: 29769–29777.
- Sali, A., and Blundell, T.L.** (1993). Comparative protein modelling by satisfaction of spatial restraints. *J. Mol. Biol.* **234**: 779–815.
- Scanlan, D.J., Ostrowski, M., Mazard, S., Dufresne, A., Garczarek, L., Hess, W.R., Post, A.F., Hagemann, M., Paulsen, I., and Partensky, F.** (2009). Ecological genomics of marine picocyanobacteria. *Microbiol. Mol. Biol. Rev.* **73**: 249–299.
- Sheta, E.A., McMillan, K., and Masters, B.S.** (1994). Evidence for a bidomain structure of constitutive cerebellar nitric oxide synthase. *J. Biol. Chem.* **269**: 15147–15153.
- Six, C., Sherrard, R., Lionard, M., Roy, S., and Campbell, D.A.** (2009). Photosystem II and pigment dynamics among ecotypes of the green alga *Ostreococcus*. *Plant Physiol.* **151**: 379–390.
- Söding, J., Biegert, A., and Lupas, A.N.** (2005). The HHpred interactive server for protein homology detection and structure prediction. *Nucleic Acids Res.* **33** (Web Server issue): W244–W248.
- Sørensen, H.P., and Mortensen, K.K.** (2005). Advanced genetic strategies for recombinant protein expression in *Escherichia coli*. *J. Biotechnol.* **115**: 113–128.
- Stuehr, D.J., Cho, H.J., Kwon, N.S., Weise, M.F., and Nathan, C.F.** (1991). Purification and characterization of the cytokine-induced macrophage nitric oxide synthase: An FAD- and FMN-containing flavoprotein. *Proc. Natl. Acad. Sci. USA* **88**: 7773–7777.
- Thompson, J.D., Gibson, T.J., Plewniak, F., Jeanmougin, F., and Higgins, D.G.** (1997). The CLUSTAL_X windows interface: Flexible strategies for multiple sequence alignment aided by quality analysis tools. *Nucleic Acids Res.* **25**: 4876–4882.
- Tillmann, U.** (2004). Interactions between planktonic microalgae and protozoan grazers. *J. Eukaryot. Microbiol.* **51**: 156–168.
- Valderrama, R., Corpas, F.J., Carreras, A., Fernández-Ocaña, A., Chaki, M., Luque, F., Gómez-Rodríguez, M.V., Colmenero-Varea,**

- P., Del Río, L.A., and Barroso, J.B.** (2007). Nitrosative stress in plants. *FEBS Lett.* **581**: 453–461.
- Vardi, A., Bidle, K.D., Kwityn, C., Hirsh, D.J., Thompson, S.M., Callow, J.A., Falkowski, P., and Bowler, C.** (2008). A diatom gene regulating nitric-oxide signaling and susceptibility to diatom-derived aldehydes. *Curr. Biol.* **18**: 895–899.
- Vardi, A., Formigini, F., Casotti, R., De Martino, A., Ribalet, F., Miralto, A., and Bowler, C.** (2006). A stress surveillance system based on calcium and nitric oxide in marine diatoms. *PLoS Biol.* **4**: e60.
- Wang, Z.Q., Lawson, R.J., Buddha, M.R., Wei, C.C., Crane, B.R., Munro, A.W., and Stuehr, D.J.** (2007). Bacterial flavodoxins support nitric oxide production by *Bacillus subtilis* nitric-oxide synthase. *J. Biol. Chem.* **282**: 2196–2202.
- Wiederstein, M., and Sippl, M.J.** (2007). ProSA-web: Interactive web service for the recognition of errors in three-dimensional structures of proteins. *Nucleic Acids Res.* **35** (Web Server issue): W407–W410.
- Xu, J., Xu, X., and Verstraete, W.** (2000). Adaptation of *E. coli* cell method for micro-scale nitrate measurement with the Griess reaction in culture media. *J. Microbiol. Methods* **41**: 23–33.
- Yamasaki, H., Sakihama, Y., and Takahashi, S.** (1999). An alternative pathway for nitric oxide production in plants: New features of an old enzyme. *Trends Plant Sci.* **4**: 128–129.